Cyanosilylation of aldehydes catalyzed by a porous metal-organic framework containing a coordinatively unsaturated Zn(II) center and its anticancer activity in human osteogenic sarcoma

Yu-Xu Li, Gang Chen, Qiang Xiao, Jin-Hui Cheng, Zhi-Sheng Long, Liang Deng, Ling Ma & Fei-Peng Gong

View supplementary material

Published online: 05 Sep 2019.

Submit your article to this journal

View related articles

View Crossmark data

Check for updates

Cyanosilylation of aldehydes catalyzed by a porous metal-organic framework containing a coordinatively unsaturated Zn(II) center and its anticancer activity in human osteogenic sarcoma

Yu-Xu Li[a†], Gang Chen[a†], Qiang Xiao[a], Jin-Hui Cheng[a], Zhi-Sheng Long[a], Liang Deng[a], Ling Ma[b] and Fei-Peng Gong[a]

[a]Department of Orthopedics, Jiangxi Provincial People's Hospital, Nanchang, China; [b]Department of Cardiology, The 940th Hospital Joint Logistics Support Force of Chinese People's Liboration Army, Lanzhou, China

ABSTRACT

Solvothermal reaction of $Zn(NO_3) \cdot 6H_2O$ with the tripodal ligand 1,3,5-tris(4-carboxyphenyl)benzene (H_3BTB) afforded a highly porous metal-organic framework (MOF) $\{[Zn_3(BTB)_2(H_2O)_2] \cdot 7DMF\}_n$ (**1**). The resulting activated **1a** exhibits BET surface areas of $1021 \, m^2 \, g^{-1}$ with a pore size distribution around 11.8 Å, which was further applied in the cyanosilylation of aldehydes under solvent-free conditions. The experimental results show that, using **1a** as the catalyst, both aliphatic and aromatic aldehydes were efficiently transformed to cyanohydrin trimethylsilyl ether. Meanwhile, significant size selectivity and electronic effects have also been observed. Then, we evaluated the anticancer activity of the synthesized compound **1a** on six different kinds of cancer cell lines, including HeLa, CHO, HepG2, MG-63, MAD-MB-435, and BEAS-2B. CCK-8 results indicated **1a** showed excellent inhibitory effect on cell proliferation, especially on the MG-63 human osteogenic sarcoma cells. Next, a transwell assay was performed to detect the migration and invasion activity of MG-63 cells after compound **1a** treatment.

1. Introduction

Cyanohydrins play an important role in chemistry and biology [1]. They are widely employed as versatile building blocks for fine chemicals, agrochemicals, and pharmaceuticals, i.e. α-hydroxy acids, β-amino alcohols, etc. Generally, the addition of cyanide to carbonyl compounds represents one of the fundamental approaches for their preparation and has frequently been at the forefront of synthetic chemistry [2]. In consideration of easy and safe management, the most often used cyanide source is trimethylsilyl cyanide (TMSCN), which allows the cyanohydrins to be prepared as the corresponding trimethylsilyl ether [3–5]. Over the past several decades, a variety of activators or promoters have been reported for this transformation. In light of pressure to develop environmentally benign systems, organocatalysts have grown rapidly in promoting the cyanosilylation of carbonyl compounds with TMSCN. Although organocatalytic systems comply with some features of green chemistry, they are still encountered with tedious separation and recycling problems in practical applications [6]. Therefore, a mild, efficient and environmentally friendly synthetic method for cyanohydrin trimethylsilyl ethers is still highly desirable.

As an emerging class of porous crystalline material, metal-organic frameworks can be synthesized from metal ions and organic multi-dentate ligands under mild conditions [7–9]. These materials have certain desirable properties such as large surface area, different pore volumes, and their distribution, size, and shape of pores, etc., that can be controlled via ligand design as well as choice of metal ion(s). Furthermore, compared with other heterogeneous catalysts, the ordered nature of MOFs allows for

precise characterization of catalytic sites through X-ray diffraction studies, which makes their catalysis center and the pore surroundings resolvable [10]. The vacant coordination sites in MOFs can activate carbonyl compounds for nucleophilic addition in a manner similar to Lewis acids. Since the first example of a MOF catalyzed reaction was reported by Fujita *et al.*, dozens of papers concerning MOF-based heterogeneous catalysis have been thus far published [11–13]. More specifically, Kaskel and co-workers demonstrated that pure MIL-101(Cr) is an efficient catalyst for the cyanosilylation of benzaldehyde [14]. Long *et al.* used a Mn(II)-based MOF as a catalyst for cyanosilylation reactions [15]. It is proposed that the Mn(II) ions exposed on the surface of the framework act as Lewis acid sites. Despite the progress on MOFs catalyzed reactions, there has been little focus on the investigation of cyanosilylation reactions using porous Zn(II)-based MOFs with unsaturated Zn(II) centers as the heterogeneous catalyst since $ZnCl_2$ has already been proved as an effective homogeneous catalyst for cyanosilylation reactions [16]. On the other hand, the construction of metal-based anticancer drugs has received great attention in the past few decades since the clinical success of cisplatin [17]. To overcome the toxicities of platin-based anticancer drugs, many low cost first-row transition metal ions have been studied as coordination centers of potential anticancer agents [18]. Zinc is an important biometal, essential for life, which is second only to iron in terms of its concentration in biological systems and is present in more than 300 enzymes of living organisms. Recent studies provided compelling evidence that Zn(II) derivatives have proved to be potential anticancer agents with low *in vivo* toxicity, low side effects and perhaps new modes of action and cellular targets compared with the classical metallodrugs [19–21]. In this study, a new porous metal-organic framework $\{[Zn_3(BTB)_2(H_2O)_2]\cdot 7DMF\}_n$ (**1**), along with its activated sample **1a** was prepared, and their catalytic cyanosilylation performances and anticancer activity were studied.

2. Experimental

2.1. Materials and instrumentation

The H_3BTB ligand was obtained from the Jinan Henghua Sci. & Tec. Co. Ltd. and used without purification. $Zn(NO_3)_2 \cdot 6H_2O$, TMSCN, and aldehydes were purchased from Beijing Bailingwei Chemical Reagent Company (Beijing, China) in analytical grade. The solvents used in this work were purchased from Tianjin Fuchen Chemical Reagents Company Limited (Tianjin, China). Elemental analyses (C, H, and N) were determined with a Perkin-Elmer 240 elemental analyzer. Thermogravimetric analysis was carried out on a NETSCHZ STA-449C thermo-analyzer with a heating rate of $10°$ min^{-1} under a nitrogen atmosphere. Powder X-ray diffraction (PXRD) analyses were recorded on a Bruker AXS D8 advanced automated diffractometer with Cu-Kα radiation.

2.2. Cell and culture condition

Human cervical cancer cell line HeLa, Chinese hamster ovary cell CHO, the liver cancer cell line HepG2, human osteogenic sarcoma cell line MG-63, breast cancer cell line MDA-MB-435S, and the normal human lung epithelial cell line BEAS-2B were

purchased from Biological Sciences (Shanghai, China), CAS. The HeLa, HepG2, MG-63, MDA-MB-435S, and BEAS-2B cells were cultured in Dulbecco's Modified Eagle's Medium (DMEM) medium, and CHO cells were cultured in 1640 culture medium (Gibco, Carlsbad, CA, USA). Both the DMEM and 1640 culture media were supplemented with 10% heated-fetal bovine serum, $100 \, U \, mL^{-1}$ penicillin-streptomycin solution (HyClone, UT, USA). The above cells were cultured in an incubator at $37\,°C$, 5% CO_2.

2.3. Synthesis of catena-[bis(µ-1,3,5-tris(4-carboxylatophenyl)benzene)-(µ-hydrate)-trizinchepta-N,N-dimethylformamide solvate] (1)

A mixture of 1,3,5-tris(4-carboxyphenyl)benzene (H_3BTB) (15.4 mg, 0.035 mmol) was added to 3 mL of 1:1 (v/v) H_2O/dimethylformamide (DMF) solution, then $Zn(NO_3)_2 \cdot 6H_2O$ (40.2 mg, 0.135 mmol) and three drops of concentrated nitric acid were added. The solutions were mixed well in a 20 mL glass scintillation vial, and then heated to $90°$ and kept at that temperature for 3 days. After cooling slowly to room temperature, colorless block crystals were isolated with 36% yield (10 mg) based on H_3BTB. Anal. Calcd (%) for **1** $C_{75}H_{83}N_7O_{21}Zn_3$: C, 55.79; H, 5.18; N, 6.07%. Found: C, 55.91; H, 5.42; N, 6.24%. Prominent FT-IR peaks for **1** (KBr pellet, cm^{-1}): 3468(m), 2965(m), 2874(m), 2322(w), 2302(w), 1612(s), 1472(m), 1369(m), 1121(s), 1019(m), 934(s), 817(s), 779(s), 708(m).

2.4. X-ray crystallography

Single-crystal X-ray crystal data of **1** were collected on a computer-controlled Oxford Xcalibu E diffractometer with enhanced (Mo) X-ray Source ($\lambda = 0.71073\,\text{Å}$) at room temperature. The data collection was performed using the CrysAlisPro software (version: 1.171.36.32) and then reduced to HKL file format using the same software [22]. Empirical absorption correction was performed using spherical harmonics, implemented in SCALE3 ABSPACK scaling algorithm [23]. The structure was solved by SHELXT [24] and then refined using the SHELXL [25] embedded in the OLEX2 software package [26]. All non-hydrogen ions were refined anisotropically and all H ions were generated in their ideal locations. Crystallographic data and refinement details are summarized in supplementary Table S1, and selected bond distances and angles for **1** are given in supplementary Tables S2 and S3 in the ESI.

2.5. Catalytic test for cyanosylation reaction

A suspension of an aldehyde (1.0 mmol), trimethylsilyl cyanide (TMSCN, 2.0 mmol) and catalyst (0.5 mol %, **1** or **1a**) was placed in a Schlenk tube under a nitrogen atmosphere and then the mixture was stirred at room temperature under solvent-free conditions. After that, the catalyst was removed by centrifugation and then washed quickly with ethyl acetate. The conversion of aldehydes was determined by gas chromatography (GC, Agilent 7890A) analysis.

2.6. Cell viability measurement

For the cell viability detection, the cell counting kit-8 (CCK-8) assay (Sigma-Aldrich, USA) was performed according to the manuscript's protocols with a little modification. In brief, the cancer cells and BEAS-2B normal cells in the logarithmic growth phase cancer cells were seeded into 96-well plates with the final concentration of 1×10^4 cells per mL, and the cells were incubated in an incubator at 37°, 5% CO_2 for 12 h. When the cells reached the confluence of 70–80%, the serial dilutions of **1a** (0, 2.5, 5, 10, 25, 50, 100, and 200 μg mL^{-1}) were exposed to cells for 24 h treatment at 37°, 5% CO_2. Cisplatin was used as the positive control drug added into wells for the same treatment. After treatment, the culture medium was discarded and fresh medium supplemented with 100 μL CCK-8 medium was added into the wells for another 4 h of cultivation. Finally, the optical density (OD) at 450 nm of each group was measured by enzyme immunoassay analyzer (Bio-Rad, USA). Each group had three repeats.

2.7. Transwell assays

The migration and invasion ability of cancer cells and BEAS-2B normal cells after being treated with compound **1a**, free ligand (H_3BTB ligand) and metal ion ($Zn(NO_3)_2 \cdot 6H_2O$) was determined. The free ligand and metal ion were used at the concentration of 0.5 mol%, and 1:1 (v/v) H_2O/dimethylformamide (DMF) was used as the solvent. Results were detected by transwell assay as described previously with some modifications. In short, for cell the migration assays, 24-well transwell chambers (Corning, NY, USA) were placed into cell culture plates before experiments. Then, the MG-63 human osteogenic sarcoma cells were planted onto the upper chamber in DMEM culture medium without FBS, and DMEM culture medium with 10% FBS was added into the lower chamber. After 24 h of culture at 37°, 5% CO_2, the cells remaining on the upper membrane were wrapped carefully, and the cells on the lower surface of the membrane were stained with 0.5% crystal violet. The numbers of cells on the lower surface of the membrane were quantified with a microscope. For the cell invasion assay, the 24-well transwell chambers used in this experiment were pre-coated with matrigel matrix (BD Biosciences, NJ, USA) and then the measurement was conducted according to the above protocols.

3. Results and discussion

3.1. Crystal structure of 1

The single-crystal X-ray diffraction study reveals that **1** belongs to the orthorhombic space group *P*nma and shows a 3-D framework structure composed of the triangular prism-shape {Zn$_3$(CO$_2$)$_6$(H$_2$O)$_2$} as the secondary building unit (SBU). The asymmetric unit of **1** is composed of one and a half Zn(II) ions, one-half μ_3-bridging water molecule, one-half μ_1-coordinating water molecule, one fully deprotonated BTB^{3-} ligand and three disordered lattice DMF molecules as revealed via the TGA analyses, all of which contribute to a neutral framework structure. The two Zn(II) ions in the molecular unit show different coordination environments. The Zn1 ion located on the inversion center is six-coordinate by four carboxylate O ions, one μ_3-bridging water molecule

and one μ_1-coordinating water, forming a distorted octahedral geometry. The tetrahedral coordination geometry of Zn2 ions is finished by four carboxylate O ions from four different BTB^{3-} ligands. The Zn1-O bond distances are in the range of 2.053(2) to 2.109(3) Å and the Zn2–O bond distances are in the region of 1.913(4) to 2.011(2) Å, which are all comparable with those observed in other Zn(II)-based MOFs based on the same H$_3$BTB ligand [27, 28]. It could be found that the distances for the Zn1–O bonds are larger than those for the Zn2–O bonds, which might be due to their different coordination geometries. Two Zn2 ions and one Zn1 ion are coupled together via the μ_3-bridging water molecule along with four bidentate chelating and two monodentate coordination carboxylic groups to afford the {Zn$_3$(CO$_2$)$_6$(H$_2$O)$_2$} SBU whose axis position is occupied via the coordinated water molecule (Figure 1). As for the BTB^{3-} ligand, it acts as a five-connected node in which the carboxylic groups are in the μ_5-η^0:η^1:η^1:η^1:η^1:η^1 coordination mode. Such a coordination pattern of BTB^{3-} ligand has been reported in other MOFs [29]. The connection of the {Zn$_3$(CO$_2$)$_6$(H$_2$O)$_2$} SBU with the BTB^{3-} ligand leads to the formation of a highly porous 3-D framework with 2-D pores along the a and b axes. The void space for the single network is large enough for the accommodation of another identical network to form a twofold interpenetrated framework (Figure 1(c)). Although twofold interpenetrated, the framework of **1** still holds considerable solvent accessible voids of 63.3% as calculated via the software PLATON. Together with the large solvent accessible void, there also exist 2-D rhombic
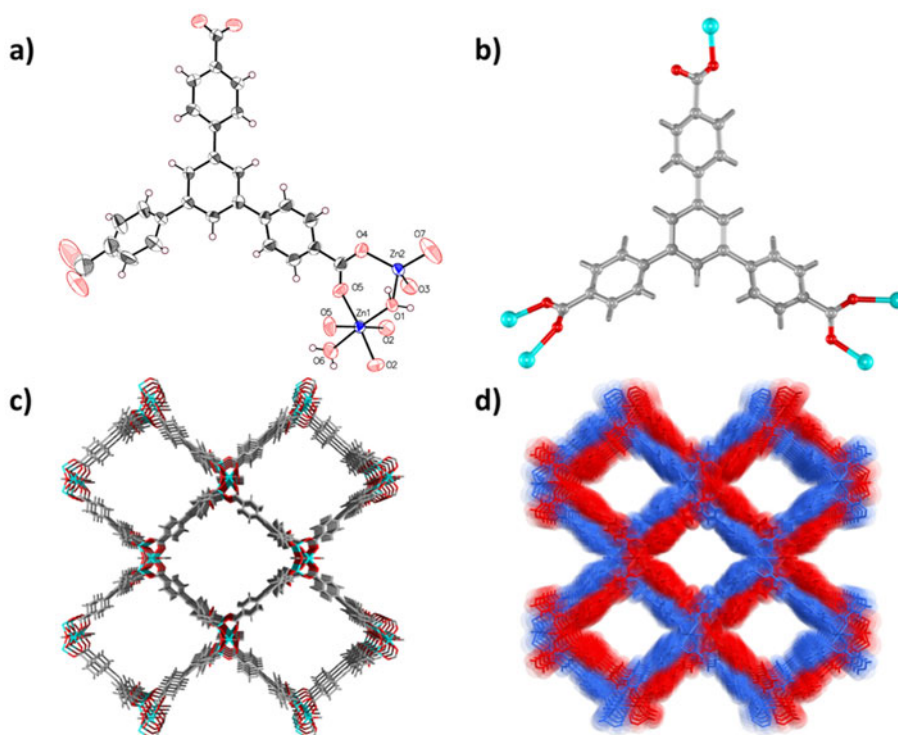

Figure 1. (a) View of the asymmetric unit of **1** and the coordination environments of Zn(II) ions. (b) The coordination mode of the organic ligand. (c) The 3-D framework of **1**. (d) A view of twofold interpenetration.

channels running along the a and b axes with a window size of 11.95×9.28 Å^2 whose vertices are filled with the water coordinated Zn(II) centers (Figure 1(d)).

3.2. PXRD, TGA, and BET analyses

To check the phase purity of the bulk as-prepared complex **1**, crystalline samples in different reaction systems were collected and the corresponding PXRD pattern was collected at room temperature. PXRD of the as-synthesized **1** gives fully matched diffraction patterns compared to the simulated patterns from single-crystal data, reflecting good phase purity, and well-defined structure (Figure 2). Thermal stability of **1** was determined by thermogravimetric analysis (TGA). As shown in Figure 2(b), the dehydration processes of **1** started from 120°. With further heating, it showed fast and continuous weight loss of 33.2% until 250°, which can be assigned as the removal of one coordinated H_2O and seven lattice DMF molecules per unit (calcd 32.8%). Then, it showed a slow weight loss and decomposed after 420° (Figure 2(b)). The third decomposition step was detected in the temperature range of 550–610°; this could be attributed to decomposition of the organic ligand giving off CO_2 and H_2O gases leaving ZnO as the final product (JCPDS: 36-1451) [30]. To evaluate the permanent porosity, the as-synthesized samples of **1** were immersed in acetone for 3 days to remove the high-boiling DMF solvents, which were further outgassed overnight under vacuum at
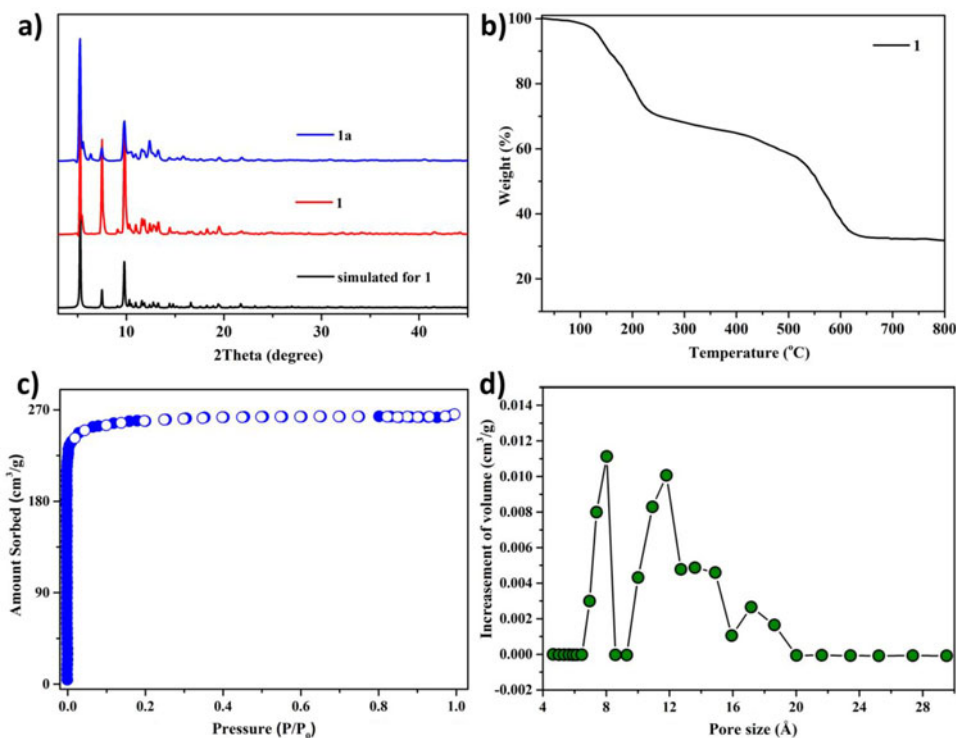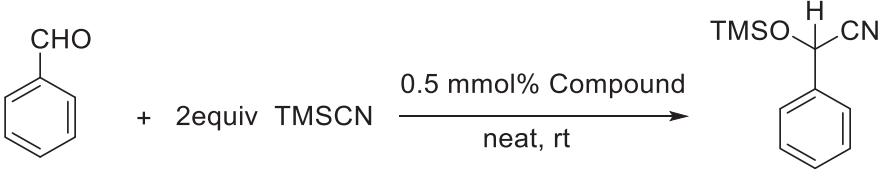

Figure 2. (a) The PXRD patterns for **1** and **1a**. (b) The TGA curve for **1**. (c) The 77 K N_2 sorption isotherm for **1**. (d) The measured pore size distribution (PSD) curve based on the density-functional theory (DFT) method.

100° for 1 day to afford the activated **1a**. The PXRD pattern of **1a** collected at room temperature reflected its good match with the one of as-prepared samples, indicating **1** kept its framework integrity in the solvent exchange and the activation processes [31]. N_2 sorption isotherms at 77 K of **1a** display the typical type-I sorption behavior with a maximum uptake capacity of 268 cm^3 g^{-1}, illustrating a typical crystalline microporous nature for **1a**. Based on the N_2 sorption isotherm, the calculated Langmuir and BET surface areas of **1a** are 1148 and 1021 m^2 g^{-1}. The measured pore size distribution (PSD) curve based on the density-functional theory (DFT) method shows the main pore sizes of 8.03 and 11.8 Å, which is related to the window size for the channels running along the *a* and *b* axes (Figure 2(d)).

3.3. Catalytic activity

The cyanosilylation reaction between TMSCN and benzaldehyde was chosen as the model reaction system to assess the catalytic properties of **1a** with the untreated complex **1** as the reference. As shown in Table 1, the reaction without catalyst resulted in only 13% conversion of benzaldehyde. However, in the presence of 0.5 mol% of catalyst, we were pleased to find that the addition of the MOF can accelerate this reaction under solvent-free conditions and **1a** gives a higher conversion at the same time intervals than that of **1**. Since **1** and **1a** are constructed by the same building blocks but with different metal sites, the different reaction rate is mainly related with the nature of functional sites in the catalysts. Coordinatively unsaturated metal ions can act as Lewis acid sites and coordinate with the carbonyls, which could activate the carbonyls and facilitate the nucleophilic attack by the TMSCN. Complex **1** shows a much higher catalytic activity than that of the blank experiment, which might be due to the release of DMF and coordinated water molecules from the cavities, and a similar observation has also been reported in the literature [32]. When using the $Zn(NO_3) \cdot 6H_2O$ as the catalyst, only 39% yield was observed, which indicates that the open Zn(II) center is more cationic and a stronger Lewis acid than mononuclear $Zn(NO_3) \cdot 6H_2O$. To study the effect of substituent

Table 1. The results for the catalytic cyanosilylation of aldehydes in the presence of different catalysts.

Entry	Catalyst	Time (h)	Conv.[a] (%)
1	none	3 h	13
2	1	3 h	43
3	1a	3 h	98
4	$Zn(NO_3)_2 \cdot 6H_2O$	3 h	39

[a]Conversion determined by GC.

Table 2. The results for the catalytic cyanosilylation of aldehydes in the presence of different catalysts.
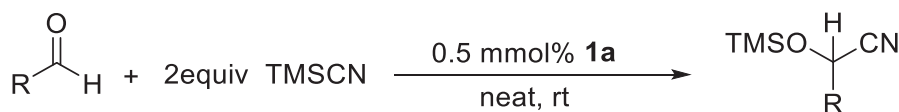
| Entry	R	Time (h)	Yield^a (%)
1	(CH$_3$)$_2$CH	3 h	100
2	n-C$_7$H$_{15}$	3 h	100
3	C$_6$H$_5$	3 h	98
4	2-NO$_2$C$_6$H$_4$	3 h	100
5	3-OCH$_3$C$_6$H$_4$	3 h	89
6	2-Furanyl	3 h	92
7	1-Naphthyl	3 h	21

^{a}Conversion determined by GC.

groups on the cyanosilylation reaction, various aldehydes were used as the reaction substrates. As indicated in Table 2, both aliphatic and aromatic aldehydes are well tolerated with this reaction protocol and could be converted to the corresponding O-trimethylsilyl cyanohydrin in good yields. Aliphatic aldehydes and benzaldehydes bearing electron-withdrawing groups on aromatic rings proceed smoothly to give the respective cyanosilylation products with high yields. Benzaldehydes bearing electron-donating groups react much more slowly than benzaldehydes with electron-withdrawing groups. To further probe the size selectivity of **1a**, larger size aromatic 1-naphthaldehydes were used as substrates. It is with no surprise that significant size selectivity is observed with **1a** and yields for both substrates decrease dramatically as compared with benzaldehyde in the following order: benzaldehyde > 1-naphthaldehyde. The relative substrate dimensions indicated that the pore windows of **1a** are large enough to allow benzaldehyde (8.21 × 5.83 Å^2) to diffuse swiftly through the channels to reach the catalytic active centers. In contrast, a significant decrease in reaction rate was observed for larger size substrates. The yield for 1-naphthaldehyde (12.69 × 8.29 Å) reduced to 21% under similar conditions. As evident for the above results, **1a** demonstrated its size selectivity and applicable substrate dimensions.

Based on the experimental results and previously reported results, a plausible reaction mechanism is proposed to illustrate the process of **1a′** catalyzed cyanosilylation reaction [11–14]. The labile water molecules in the channels of **1** were removed by heating to expose the unsaturated metal sites previously. The aldehydes were activated by the coordinatively unsaturated Zn centers to react with TMSCN (Scheme 1). The products were replaced by aldehydes, and the catalysts continued to activate the aldehydes in the next catalytic cycle.

3.4. Compound 1a showed special inhibitory effect on MG-63 human osteogenic sarcoma cells

After the design and synthesis of **1a** with its novel structure, the anticancer activity of **1a** was further explored. In this research, the CKK-8 assay was conducted to detect
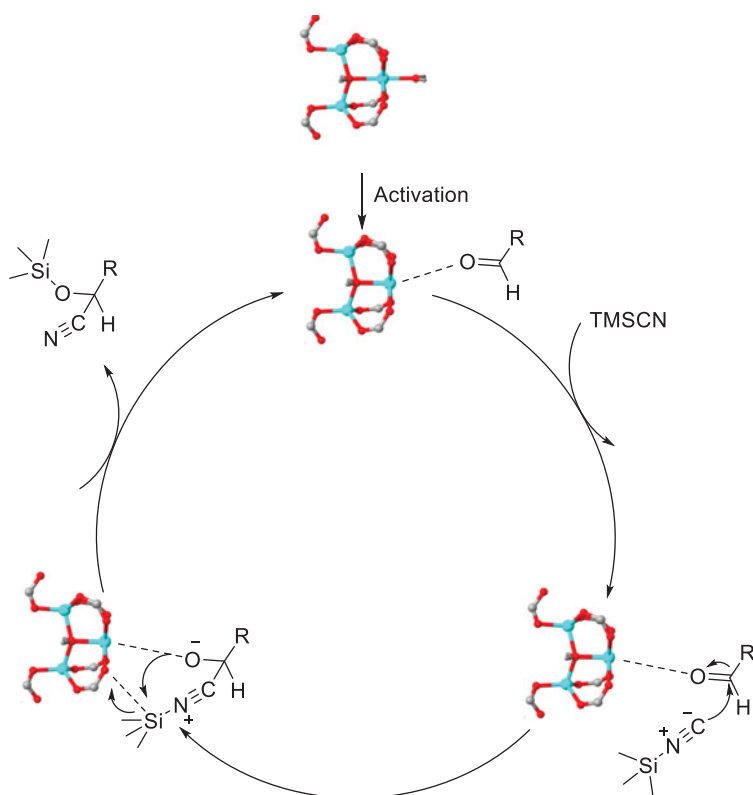
Scheme 1. Proposed mechanism for the cyanosilylation reaction of carbonyl compounds catalyzed by **1a**.

the cell viability of different types of cancer cells after serial dilution treatment with **1a**. As the results show in Figure 3, **1a** exhibited no inhibitory effect on MDA-MB-435S cancer cells, moderate inhibition on HeLa, CHO, HepG2 cancer cells, and excellent inhibition on MG-63 cancer cells. The IC_{50} of **1a** on MG-63 cancer cells is $2.5 \pm 0.3 \,\mu g \,mL^{-1}$ (Table 3), which is significantly lower than the IC_{50} of other cancer cells, indicating **1a** showed a much better inhibition on MG-63 cancer cells compared with other cells. Based on this data, the MG-63 cell line was selected for research about the anticancer activity of **1a**.

3.5. MG-63 cell proliferation, migration, and invasion after compound 1a treatment

In the previous study, we confirmed that **1a** showed special inhibition on the MG-63 human osteogenic sarcoma cells, compared with other cells. Next, we further explored the inhibitory effect of **1a** on cancer cell proliferation, migration, and invasion ability. The MG-63 cell proliferation was assessed by CCK-8. After treated with **1a** at 2.5 mg mL^{-1} for 48 h, the cell proliferation curves were plotted. As the results show in Figure 4(a), we can see the compound **1a** treatment significantly reduced the proliferation of cancer cells, in comparison with other control groups, free ligand, and metal ion treatment groups ($p < .005$). Besides, transwell assay was performed to explore the effect
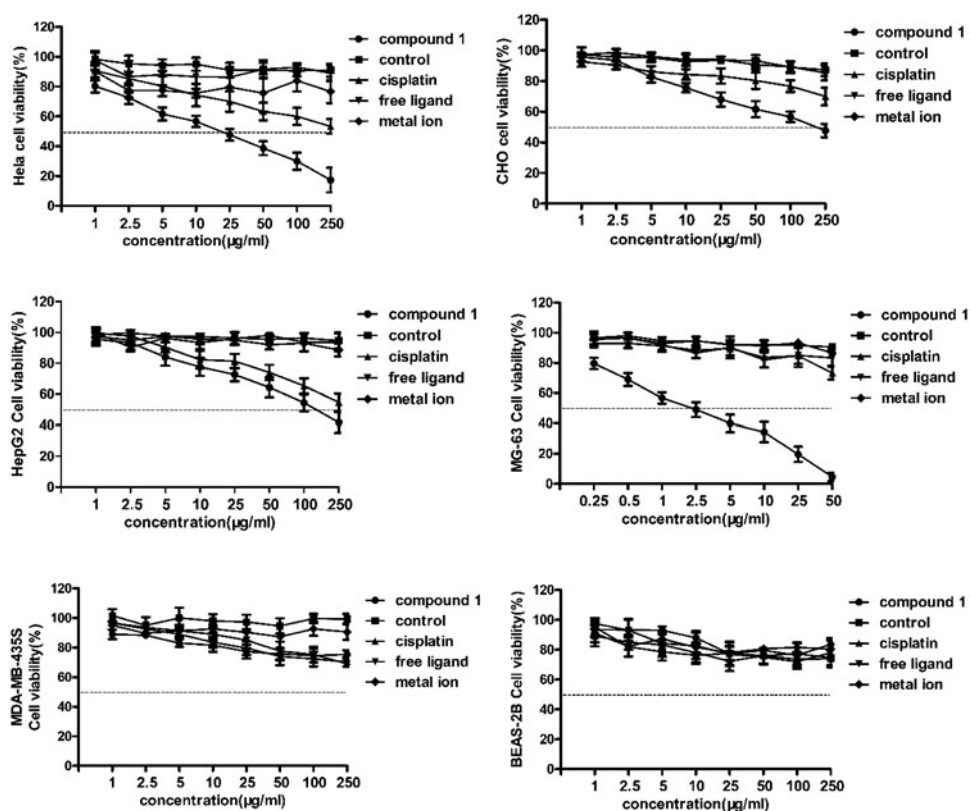
Figure 3. The inhibition of **1a** on different kinds of cancer cell viability. Different types of cancer cell lines were exposed to serial concentrations of **1a**. A CCK-8 detection kit was used to measure the cell viability, and the IC_{50} was calculated according to the results. All experiments were performed at least three times.

Table 3. IC_{50} Values of compound on cancer cells.

IC_{50} ($\mu g\ mL^{-1}$)	HeLa	CHO	HepG2	MG-63	MAD-MB-435	BEAS-2B
1a	24.5 ± 1.6	>250	120 ± 3.4	2.5 ± 0.3	>250	>250
Cisplatin	>250	>250	>250	>250	>250	>250
Free ligand	>250	>250	>250	>250	>250	>250
Metal ion	>250	>250	>250	>250	>250	>250

of **1a** on cancer cells migration and invasion ability. From the results exhibited in Figure 4(b) and (c), we found that the number of migrated and invaded MG-63 cancer cells could be significantly reduced by **1a**, and the free ligand and metal ion had no effect on the cell migration and invasion ability. Above all, we can draw this conclusion, **1a** significantly inhibited MG-63 cells proliferation, migration, and invasion ability.

4. Conclusion

We have prepared a new Zn(II)-based porous metal-organic framework containing abounding coordinatively unsaturated Zn(II) centers. The structural characterization
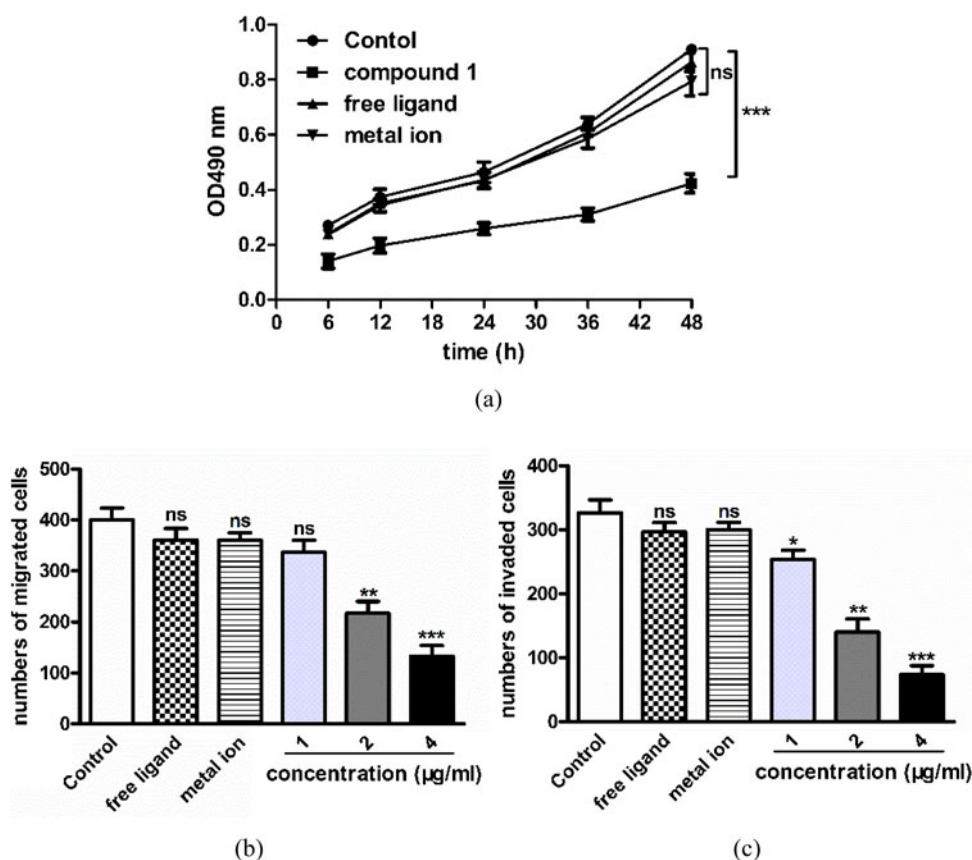
Figure 4. Reduced MG-63 cancer cells proliferation, migration, and invasion after compound 1a treatment. MG-63 cells were exposed to serially dilutions of 1a. (a) Cell proliferation determined by cell counting kit-8 assay. (b, c) The cell migration and invasion capability examined by transwell assay. There is a significant difference with $p < .05$. All experiments were performed in triplicate.

based on single-crystal data collected at 298 K reveals that **1** shows a 3-D framework structure with 1-D nano-sized channels along the *a* axis, which are functionalized with high density of unsaturated Zn(II) centers. Due to its high BET surface areas and large pore aperture, the activated MOF was studied as a catalyst for the cyanosilylation of aldehydes under solvent-free conditions. The experimental results show that using **1a** as the catalyst, both aliphatic and aromatic aldehydes were efficiently transformed to cyanohydrin trimethylsilyl ether. Meanwhile significant size selectivity and electronic effects have also been observed. To evaluate the inhibitory effect of **1a** on cancer cells, HeLa, CHO, HepG2, MG-63, MDA-MB-435S, and BEAS-2B cell lines were used for the CCK-8 assay. Results indicated the excellent anticancer activity of **1a** on MG-63 human osteogenic sarcoma cell line, with the IC_{50} of $2.5 \pm 0.3\,\mu g\ mL^{-1}$. Subsequently, the influence of **1a** on MG-63 cells proliferation, migration and invasion capability was examined using transwell assay. Through the above experiments, we draw the conclusion that **1a** inhibited the MG-63 proliferation, migration, and invasion, indicating the potential of being a candidate for human osteogenic sarcoma treatment.

Disclosure statement

No potential conflict of interest was reported by the authors.

References

[1] F. Ortega-Caballero, C. Rousseau, B. Christensen, T.E. Petersen, M. Bols. *J. Am. Chem. Soc.*, **127**, 3238 (2005).
[2] Y.N. Belokon', B. Green, N.S. Ikonnikov, M. North, T. Parsons, V.I. Tararov. *Tetrahedron*, **57**, 771 (2001).
[3] W.J. Greenlee, D.G. Hangauer. *Tetrahedron Lett.*, **24**, 4559 (1983).
[4] M. Bandini, P.G. Cozzi, P. Melchiorre, A. Umani-Ronchi. *Tetrahedron Lett.*, **42**, 3041 (2001).
[5] D.A. Evans, G.L. Carroll, L.K. Truesdale. *J. Org. Chem.*, **39**, 914 (1974).
[6] W. Wang, M. Luo, J. Li, S.A. Pullarkat, M. Ma. *Chem. Commun. (Camb.)*, **54**, 3042 (2018).
[7] X. Feng, Y.Q. Feng, N. Guo, Y.L. Sun, T. Zhang, L.F. Ma, L.Y. Wang. *Inorg. Chem.*, **56**, 1713 (2017).
[8] X. Feng, R. Li, L. Wang, S.W. Ng, G. Qin, L. Ma. *CrystEngComm*, **17**, 7878 (2015).
[9] X. Feng, Y.-Q. Feng, L. Liu, L.-Y. Wang, H.-L. Song, S.-W. Ng. *Dalton Trans.*, **42**, 7741 (2013).
[10] D.M. Chen, J.Y. Tian, Z.W. Wang, C.S. Liu, M. Chen, M. Du. *Chem. Commun.*, **53**, 10668 (2017).
[11] O. Ohmori, M. Fujita. *Chem. Commun.*, **55**, 1586 (2004).
[12] A. Bhunia, S. Dey, J.M. Moreno, U. Diaz, P. Concepcion, K. Van Hecke, C. Janiak, P. Van Der Voort. *Chem. Commun. (Camb.)*, **52**, 1401 (2016).
[13] X. Cui, M.C. Xu, L.J. Zhang, R.X. Yao, X.M. Zhang. *Dalton Trans.*, **44**, 12711 (2015).
[14] A. Henschel, K. Gedrich, R. Kraehnert, S. Kaskel. *Chem. Commun.*, **5**, 4192 (2008).
[15] S. Horike, M. Dinca, K. Tamaki, J.R. Long. *J. Am. Chem. Soc.*, **130**, 5854 (2008).
[16] N.H. Ho, W.J. Le Noble. *J. Org. Chem.*, **54**, 2018 (1989).
[17] N. Muhammad, Z. Guo. *Curr. Opin. Chem. Biol.*, **19**, 144 (2014).
[18] K.B. Garbutcheon-Singh, M.P. Grant, B.W. Harper, A.M. Krause-Heuer, M. Manohar, N. Orkey, J.R. Aldrich-Wright. *Curr. Top. Med. Chem.*, **11**, 521 (2011).
[19] S. Mukherjee, S. Ganguly, K. Manna, S. Mondal, S. Mahapatra, D. Das. *Inorg. Chem.*, **57**, 4050 (2018).
[20] B. Fernández, I. Fernández, J. Cepeda, M. Medina-O'Donnell, E.E. Rufino-Palomares, Á. Raya-Barón, S. Gómez-Ruiz, A. Pérez-Jiménez, J.A. Lupiáñez, F.J. Reyes-Zurita, A. Rodríguez-Diéguez. *Cryst. Growth Des.*, **18**, 969 (2018).
[21] Y.P. Zhang, Z.Y. Ma, C.Y. Gao, X. Qiao, J.L. Tian, W. Gu, X. Liu, J.Y. Xu, J.Z. Zhao, S.P. Yan. *New J. Chem.*, **40**, 7513 (2016).
[22] P.R.O. CrysAlis. Agilent Technologies Ltd. [J]., Yarnton, Oxfordshire, England (2014).
[23] *SCALE3 ABSPACK: Empirical Absorption Correction, CRYSALIS-Software Package*, Oxford Diffraction Ltd., Oxford (2006).
[24] G.M. Sheldrick. *Acta Crystallogr., Sect. A*, **71**, 3 (2015).
[25] G.M. Sheldrick. *Acta Crystallogr., Sect. C*, **71**, 3 (2015).
[26] O.V. Dolomanov, L.J. Bourhis, R.J. Gildea, J.A.K. Howard, H. Puschmann. *J. Appl. Crystallogr.*, **42**, 339 (2009).
[27] D. Han, F.L. Jiang, M.Y. Wu, L. Chen, Q.H. Chen, M.C. Hong. *Chem. Commun. (Camb.)*, **47**, 9861 (2011).
[28] N. Klein, I. Senkovska, K. Gedrich, U. Stoeck, A. Henschel, U. Mueller, S. Kaskel. *Angew. Chem. Int. Ed.*, **48**, 9954 (2009).
[29] C.L. Whittington, L. Wojtas, R.W. Larsen. *Inorg. Chem.*, **53**, 160 (2014).
[30] J. Zhang, L. Sun, C. Liao, C. Yan. *Chem. Commun.*, **3**, 262 (2002).
[31] D.M. Chen, J.Y. Tian, C.S. Liu. *Inorg. Chem.*, **55**, 8892 (2016).
[32] T. Ladrak, S. Smulders, O. Roubeau, S.J. Teat, P. Gamez, J. Reedijk. *Eur. J. Inorg. Chem.*, **2010**, 3804 (2010).